Path Signature Features Revealed SSRI-Induced White Matter Morphological Reorganization in Depressions

Jiaolong Qin[1], Weihong Dong[2], Huangjing Ni[3], Zhijian Yao[4], Qing Lu[2,✉], Ye Wu[1,✉]

[1] School of Computer Science and Technology, Nanjing University of Science and Technology, Nanjing, China
wuye@njust.edu.cn
[2] School of Biological Sciences & Medical Engineering, Southeast University, Nanjing, China
luq@seu.edu.cn
[3] Key Laboratory of Brain-Machine Intelligence Technology, Ministry of Education, Nanjing University of Aeronautics and Astronautics, Nanjing, China
[4] Department of Psychiatry, the Affiliated Brain Hospital of Nanjing Medical University, Nanjing, China

Abstract. Selective serotonin reuptake inhibitors (SSRIs) are recognized as the first-line treatment for major depressive disorder; however, the characterization of their microstructural effects on white matter (WM) is still limited. This study presents a novel path signature (PS) framework to quantify longitudinal WM plasticity utilizing clinical-grade diffusion magnetic resonance imaging (MRI) data. This approach overcomes the limitations of conventional diffusion metrics, achieving a sensitivity of 1 mm^3 without requiring high-resolution imaging. By combining rough path theory with super-resolution mapping, significant SSRI-induced reorganization is found in the transverse pontine tract, left anterior limb of the internal capsule, and splenium of the corpus callosum in MDD patients. Changes in PS features in these fiber bundles and the left corticospinal tract correlate positively with reductions in the 17-item Hamilton Depression Rating Scale scores, providing preliminary evidence of a relationship between WM alterations and clinical outcomes. The findings establish PS analysis as a promising tool for detecting macrostructural plasticity in WM due to SSRIs, thereby bridging the critical gap between microstructural diffusion metrics and circuit-level reorganization, and providing a novel insight into comprehensive biomarkers for precision antidepressant therapy.

Keywords: Computational anatomy, depression, white matter.

1 Introduction

As a first-line pharmacological intervention for major depressive disorder (MDD), antidepressant medications demonstrate well-established efficacy, with selective serotonin reuptake inhibitors (SSRIs) constituting the most frequently prescribed class [1]. The SSRIs exert therapeutic effects through serotonin reuptake inhibition in white matter (WM) projections across depression-related neural circuits [2, 3]. While exten-

sive neuroimaging research has investigated SSRI-induced microstructural alterations using diffusion MRI (dMRI) metrics like fractional anisotropy (FA), a critical knowledge gap persists regarding macrostructural morphological changes in WM fiber pathways. This limitation significantly constrains the identification of robust biomarkers for predicting therapeutic responses and personalizing treatment strategies.

Tractography has advanced the study of WM through two primary methodologies: tract-based geometric analysis and voxel-based track-weighted imaging (TWI). Tract-based approaches, such as Frenet frame curvature/torsion measurements and director field theory, quantify local fiber bundle deformations (e.g., splay, bend, twist) but lack comprehensive tools for hierarchically encoding multi-scale geometric variations across entire pathways [4, 5]. Meanwhile, TWI frameworks integrate streamlined attributes (e.g., count, length, density) into voxel-level maps [6,7], yet often overlook higher-order geometric properties that are critical for characterizing complex fiber morphology [8]. Inspired by these methodological limitations, we propose leveraging path signatures (PS) to systematically characterize WM fiber geometry. The PS, initially developed through rough path theory [9, 10], provides a mathematically rigorous framework for quantifying complex morphological patterns in trajectory data through iterative integral transformations. Its unique hierarchically encoded multi-scale geometric properties have proven effective in diverse pattern recognition applications, including handwriting trajectory analysis [11, 12].

These methodological gaps are particularly salient in clinical neuroscience, such as studying antidepressant effects in MDD. Building upon these foundations, we propose a novel paradigm shift in WM analysis by applying PS methodology to longitudinal dMRI data from MDD patients undergoing SSRI treatment. Our study addresses two critical unmet needs: (1) Macrostructural sensitivity: The existing literature predominantly focuses on microstructural FA changes. At the same time, macroscopic fiber morphology, which may be more reflective of circuit-level reorganization, remains largely unexplored. (2) Analytical resolution: Conventional diffusion metrics of dMRI suffer from resolution limitations (typically 2-3 mm^3). PS-based analysis overcomes this through its differential geometry framework, which decouples morphological measurements from spatial resolution boundaries inherent to traditional approaches by extracting sub-voxel features from trajectory signatures. The novel approach has the potential to open up new avenues for understanding the impact of SSRI treatment on depression and for developing more accurate methods for predicting treatment responses.

2 Methods

2.1 Theory of PS

The essence of PS features is based on the iterated integrals in Euclidean space. For a d-dimensional path X: $[a, b] \mapsto R^d$, its signature $S(X)_{a,b}$ encodes multi-scale geometric properties as an infinite sequence of tensors, where a and b indicate start and ending points. Below, we formalize the PS construction, emphasizing its clinical applicability to WM tractography.

Let $X_t = (X_t^1, X_t^2, \ldots, X_t^d)$ denote a d-dimensional path parameterized by $t \in [a, b]$. The PS is recursively defined via iterated integrals:

First-Order Terms (Linear Displacement). Quantify net displacement along coordinate axes:

$$S(X)_{a,t}^{i} = \int_{a<s<t} dX_s^i = X_t^i - X_a^i \qquad \text{for } i = 1, \ldots, d. \tag{1}$$

These terms represent the cumulative linear movement (e.g., $\Delta x, \Delta y, \Delta z$ in a streamline).

Second-Order Terms (Curvature & Covariance). Capture pairwise interactions between displacements:

$$S(X)_{a,t}^{i,j} = \int_{a<s<t} S(X)_{a,s}^{i} dX_s^j = \int_{a<r<s<t} dX_r^i \, dX_s^j \quad \text{for } i, j = 1, \ldots, d. \tag{2}$$

Diagonal terms ($i = j$) encode self-interaction (e.g., accumulated squared displacement). Off-diagonal terms ($i \neq j$) quantify directional covariance, analogous to the curvature tensor in differential geometry [13].

Third-Order Terms (Torsion & Nonlinear Dynamics). Describe triadic interactions and non-stationary geometric properties:

$$S(X)_{a,t}^{i,j,k} = \int_{a<s<t} S(X)_{a,s}^{i,j} dX_s^k = \int_{a<q<r<s<t} dX_q^i dX_r^j \, dX_s^k \quad \text{for } i, j, k = 1, \ldots, d. \tag{3}$$

These terms resolve torsional dynamics (e.g., helical twisting in 3D fibers) and asymmetric interactions ($S^{ijk} \neq S^{ikj}$) critical for modeling WM plasticity.

General k-th Order Terms. Recursively defined as:

$$S(X)_{a,t}^{i_1,\ldots,i_k} = \int_{a<s<t} S(X)_{a,s}^{i_1,\ldots,i_{k-1}} dX_s^{i_k} \ . \tag{4}$$

The full signature $S(X)_{a,b}$ is the collection of all such terms:

$$S(X)_{a,b} = (1, \{S(X)^i\}, \{S(X)^{ij}\}, \{S(X)^{ijk}\}, \ldots) \ . \tag{5}$$

The 0-th term of the PS remains constant at 1. Theoretically, the signature of a path is an infinitely long sequence. However, in practice, we often use the first K terms of the sequence and signature terms up to the K-th order to form a new sequence for analysis. This new sequence is referred to as the K-th order truncated PS.

2.2 Construction of PS Feature Map

In this study, we opted to set the value of K at a maximum of 3 based on two primary considerations: (1) empirical evidence demonstrates that third-order PS sufficiently capture the geometric complexity required for spatial trajectory analysis; (2) these order optimally balances computational efficiency with feature discriminability, as higher-order expansions yield diminishing returns in information gain relative to their increased computational cost. Figure 1 illustrates the process of constructing PS feature maps. By utilizing a sliding window with a length encompassing three sampling points and advancing with a step of 1, we sequentially compute the PS features for each point along a fiber tract. As shown in figure 1, three sampling points within a

window, denoted as p_1, p_2 and p_3, form a local path segment. The PS feature set at point p_2 was constructed from the first- to third-order truncated PS $S_{p_1,p3}$, with the zeroth-order term excluded. This set is shown as follows:

$$S_{p_1,p_3} = (S^1_{p_1,p_3}, \ \ldots, S^3_{p_1,p_3}, S^{1,1}_{p_1,p_3}, S^{1,2}_{p_1,p_3}, \ldots, S^{3,3}_{p_1,p_3}, S^{1,1,1}_{p_1,p_3}, S^{1,1,2}_{p_1,p_3}, \ldots, S^{3,3,3}_{p_1,p_3}) \quad (6)$$

For each sampling point along WM tractography streamlines (excluding terminal points that lack valid trajectory information), we computed 39 distinct PS values corresponding to three signature orders. (1) First-order signatures (terms 1-3) quantify linear displacements along coordinate axes, capturing the most basic and primary characteristics of the path (e.g., tract elongation/contraction). (2) Second-order signatures (terms 4-12) characterize curvature and acceleration through quadratic interactions (e.g., bending in corpus callosum). (3) Third-order signatures (terms 13-39) describe higher-dimensional geometric deformations via cubic nonlinearities (e.g., spiral reorganization in cortico-cerebellar pathways). Notably, the second-order terms 4, 8, and 12 exclusively generate positive values due to their mathematical construction, which involves squared terms that eliminate directional sensitivity.

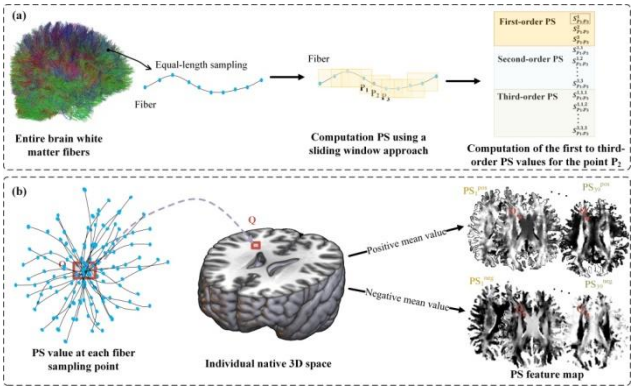

Fig. 1. The pipeline for constructing path signature (PS) feature map. (a) Schematic illustration of calculating the PS value for each point along a fiber using a sliding window. (b) After obtaining the PS values for each point on all fibers across the brain, different resolutions are set in the individual space, and the PS values are mapped to each voxel. When a voxel contains multiple sampling points (e.g., voxel Q in this figure), the positive and negative signature values are separately averaged and assigned to distinct positive and negative feature maps. This process ultimately generates multiple PS feature maps corresponding to different signature terms.

Once these 39 PS values in the entire brain are mapped back to their native 3D image space, respectively, points may be located within the same voxel of the native space. When this occurred, positive/negative PS values (representing opposing fiber trajectory directions) within each native-space voxel were separately averaged to preserve directional information as follows:

$$PS_n^{pos}(v) = \frac{1}{N_v^{pos}} \sum_{p \in v} \max(0, PS_n(p)) \quad (7)$$

$$PS_n^{neg}(v) = \frac{1}{N_v^{neg}} \sum_{p \in v} \min(0, PS_n(p)) \quad (8)$$

where v denotes a voxel and p is sampling points within v. N denotes the number of sampling points with positive or negative value within v, while n refers to specific PS terms. To simplify notation, we denote positive and negative PS maps as PS_n^{pos} and PS_n^{neg}, respectively, where the index n is defined for signature terms: first-order (1-3), second-order (4-12), and third-order (13-39).

The PS feature maps were generated at two resolutions using an open-source Python package: (1) Clinical-grade resolution (1.875 mm × 1.875 mm × 3 mm) matching raw dMRI data; (2) Super-resolution (1 mm^3 isotropic). This dual-resolution approach was implemented to visually assess potential gains in fiber tract delineation capacity within routine clinical imaging protocols.

2.3 Longitudinal Data Acquisition and Analysis

Population and Imaging Acquisition: Fifty-six MDD patients were recruited. All patients were diagnosed with a major depressive episode before treatment by at least two physicians using DSM-IV/MINI. The severity of depression was rated using the 17-item Hamilton Depression Rating Scale (HAMD-17). All patients received SSRI antidepressant therapy under standardized clinical guidelines, with dosages dynamically adjusted based on individual treatment response. Fifty-one patients (age: 31.49±8.17, 20 males) participated in baseline and 12-week post-SSRI scans. They achieved remission (HAMD-17 <7 post-treatment) and were included in the analysis. Imaging used on a 3T Siemens Verio scanner. T1-weighted image was acquired covering the whole brain with TR=1900ms, TE=2.48ms, resolution =1mm×0.9766 mm×0.9766mm. The dMRI data were acquired with a TR of 6600ms, TE=93 ms, resolution=1.875 mm×1.875 mm×3 mm. Each dMRI scan included 1 b = 0 and 270 b = 1000 s/mm^2 diffusion-weighted volumes. This study was approved by the Medical Ethics Committee of Nanjing Brain Hospital and conducted by the Declaration of Helsinki. All participants provided signed informed consent.

Image Processing and Tractography: All images underwent quality control and standardized preprocessing adhering to the principle of minimal necessary processing: alignment, centering, Gibbs ringing removal [14], and intensity correction [15]. For dMRI data, denoising [16], eddy current correction [17], EPI correction, and CNN-based brain masking[1] were applied. T1w-dMRI alignment used FSL rigid registration [17] while preserving native diffusion space. Whole-brain tractography employed the iFOD2 [18] algorithm (3 million seeds, other parameters: default). Streamlines were reduced to 1 million via SIFT filtering [19-20] and resampled at a resolution of 0.6 mm (less than half the voxel size).

Longitudinal WM Morphological Change Analysis: We obtained the average PS value of 50 WM regions based on the JHU-ICBM atlas for each MDD patient at baseline and after 12 weeks of SSRIs antidepressant treatment. Paired sample t-tests were performed to detect the differences before and after treatment, and the false

[1] github.com/pnlbwh/pnlNipype

discovery rate (FDR) was used to correct multiple comparisons. A corrected *p*-value less than 0.05 was considered to indicate a statistically significant difference.

Correlation Analysis between the Rate of Change in WM PS Feature Values and the Reduction Rate of HAMD-17 Score: The significantly altered WM regions were further investigated for their associations with the disease remission level. We formally calculated the rate of change in the PS feature value for each region $\left|\frac{\text{mean}(\text{PS}_{\text{pretreatment}})-\text{mean}(\text{PS}_{\text{posttreatment}})}{\text{mean}(\text{PS}_{\text{pretreatment}})}\right|$. Similarly, the reduction rate of the HAMD-17 score of each patient was defined as $\left|\frac{\text{HAMD}_{\text{pretreatment}}-\text{HAMD}_{\text{posttreatment}}}{\text{HAMD}_{\text{pretreatment}}}\right|$. Spearman's correlation analysis was applied to examine the correlation between these two rate values of change.

3 Results

3.1 PS Feature Map with Different Resolutions

Figure 2 compares PS_1^{pos} feature maps of a patient at original and super-resolution scales[2]. While brain-wide value distributions remain similar, super-resolution maps demonstrate markedly enhanced tissue contrast clarity. This superior resolution motivated their use in subsequent analysis.

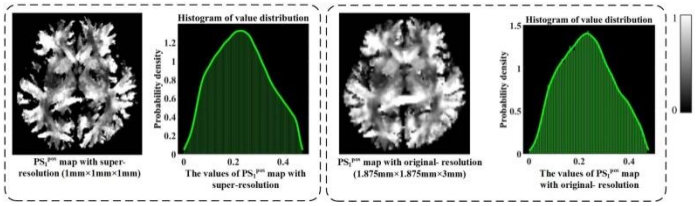

Fig. 2. Comparative transverse sections of PS_1^{pos} feature maps between original (1.875 mm × 1.875 mm × 3 mm) and super-resolution (1 mm^3) reconstructions in a representative patient.

3.2 WM Morphological Alterations in Depressions Before and After SSRI Treatment

Nine WM feature maps showed significant post-SSRI changes (PS_1^{pos}, PS_4^{pos}, PS_5^{neg}, PS_7^{neg}, PS_{14}^{neg}, PS_{25}^{pos}, PS_{26}^{pos}, PS_{36}^{pos}, and PS_{38}^{neg}), revealing five spatial patterns (Figure 3): (1) Transverse pontine tract (TPT)-dominant with FDR-corrected $p < 0.040$ (motor integration: $PS_{1,4,36}^{pos}$, PS_{38}^{neg}); (2) Left anterior limb of the internal capsule (ALIC)-clustered maps with FDR-corrected $p < 0.028$ (affective processing: $PS_{5,7}^{neg}$); (3) Multi-nodal WM with FDR-corrected $p < 0.048$ (TPT, SCC, fornix, cerebellar-capsular pathways: PS_{14}^{neg}); (4) Cortico-cerebellar with FDR-corrected $p < 0.044$ (sensorimotor-cerebellar circuits: PS_{25}^{pos}); (5) Cross-hemispheric with FDR-corrected

[2] https://github.com/qinjiaolong/PS

p < 0.045 (corpus callosum, thalamocortical connectivities: PS_{26}^{pos}). These patterns highlight SSRI-induced structural plasticity across motor, affective, and interhemispheric connectivity networks.

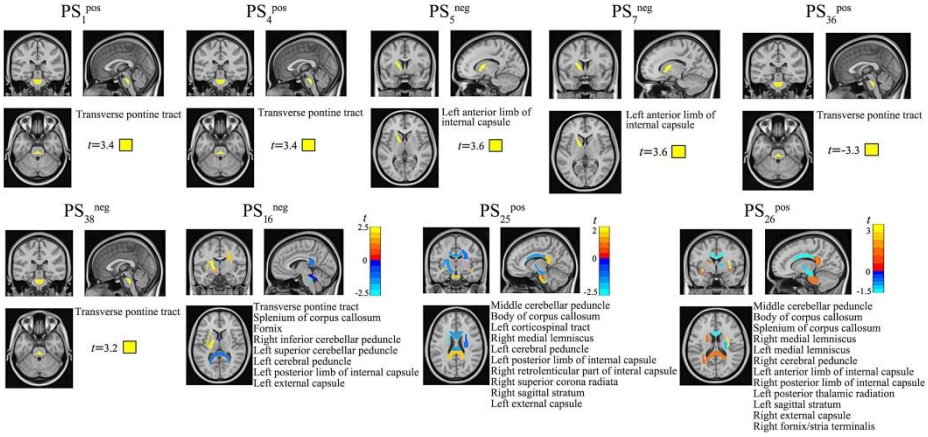

Fig. 3. The results of white matter show significant alterations before and after SSRI treatment. The bar in each subplot denotes the t-value from the paired t-test, with the name of the significantly FDR-corrected region labeled in the lower right corner. Warm colors indicate that a specific PS value was significantly higher before treatment than after. In contrast, cool colors signify that the PS value was significantly lower before treatment compared to after.

3.3 Correlation Results between the Rate of Change in PS Feature Values and the Reduction Rate of HAMD-17 Score

Figure 4 reveals significant correlations between HAMD-17 reduction rates and longitudinal changes in WM feature metrics: $\Delta PS_1^{pos}/\Delta PS_4^{pos}$ (TPT), ΔPS_{26}^{pos} (left ALIC), and ΔPS_{25}^{pos} (left CST). Increased alterations in feature values within these regions correlated with more significant symptom relief, suggesting neuroplastic adaptations in motor integration (TPT), affective processing (ALIC), and sensorimotor pathways (CST) may underpin SSRI-mediated antidepressant effects.

4 Discussion and Conclusion

Our findings demonstrate significant macrostructural WM reorganization in three key tracts following SSRI treatment: the TPT, left ALIC, and SCC. The observed morphological changes in the TPT–a crucial hub connecting cerebral motor cortices with the cerebellum [21]–align with previous reports of cerebellar system alterations in antidepressant responders [22]. While overt motor deficits do not classically characterize MDD, emerging evidence suggests subtle psychomotor disturbances may reflect cortico-cerebellar circuit dysfunction [23], potentially modulated through SSRI-induced plasticity in this pathway. The ALIC alterations are significant, given their central role in the corticostriatal-thalamic-cortical (CSTC) circuit [24], a well-established

network associated with depression. Our PS-based WM morphological measurements complement prior diffusion metric studies, which have shown FA abnormalities in this region [25–27], and extend these findings by revealing treatment-responsive macroscale geometric adaptations of fiber bundles. These structural morphological changes may underlie enhanced CSTC circuit efficiency, potentially mediating cognitive improvements and emotional regulation [28]–though direct neurophysiological validation remains necessary. The splenium changes corroborate existing findings on the commissural fiber system [29], suggesting that SSRI treatment may normalize interhemispheric communication deficits through callosal remodeling. The convergent evidence from macrostructural morphology analysis (current study) and microstructural [29] investigations strengthens the hypothesis that WM integrity restoration represents a common pathway for antidepressant efficacy.

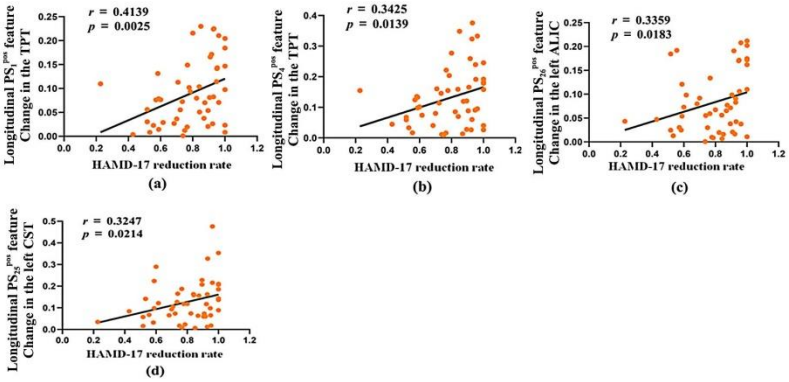

Fig. 4. The correlation results of the rate of change in average PS values within white matter regions pre- and post-SSRIs treatment with the reduction rate of the HAMD-17 score. (a), (b), (c) and (d) display the correlation results between the rate of change in the regions (i.e., PS_1^{pos} values within the transverse pontine tract (TPT), PS_4^{pos} values within the TPT, PS_{26}^{pos} values within the left anterior limb of the internal capsule (ALIC), and PS_{25}^{pos} values within the left corticospinal tract (CST)) and the reduction rate of the HAMD-17 score, respectively.

The positive correlation between longitudinal PS feature changes in the TPT, left ALIC, and left CST with HAMD-17 reduction rates provides preliminary evidence for structure-clinical outcome associations. While these tracts have been implicated in MDD pathology through diffusion metric abnormalities [30–32], our study pioneers the identification of their macroscale morphological dynamics as potential predictors of SSRI response. However, the observational nature of these correlations necessitates cautious interpretation until prospective validation establishes causal relationships.

By implementing PS-based super-resolution mapping (1 mm^3) on clinical-grade dMRI data, we achieved enhanced sensitivity in detecting subtle morphological changes that conventional dMRI metrics might overlook. This technical superiority was empirically validated through a comparison analysis. When applying identical statistical methods to the same SSRI treatment dataset, the FA map showed no significant effects (minimal FDR-corrected p = 0.067). In contrast, the PS map not only

demonstrated superior sensitivity in detecting microstructural changes but also consistently outperformed FA in gender classification tasks [33]. This technical advance addresses the resolution limitations noted in our introduction, enabling voxel-level analysis of fiber geometry through sub-voxel trajectory characterization–a critical advantage for clinical applications where high-resolution scans are often unavailable.

This study establishes PS analysis as a novel paradigm for detecting SSRI-induced WM macrostructure plasticity, bridging the critical gap between microstructural diffusion metrics and circuit-level reorganization. The key findings are as follows: (1) SSRI treatment morphological changes in motor, affective, and interhemispheric pathways; (2) Longitudinal PS alterations correlate with clinical improvement; (3) Super-resolution PS mapping enhances detection sensitivity in clinical imaging. While promising for treatment prediction, multicenter validation is required. Future research should integrate multimodal neuroimaging to develop precision biomarkers for antidepressant therapy.

Acknowledgments. This study was funded by the National Key R&D Program of China (No. 2023YFE0118600 and 2023YFF1204803), the National Natural Science Foundation of China (No. 62201265), and the Fundamental Research Funds for the Central Universities (No. NJ2024029).

Disclosure of Interests. The authors declare no competing interest in this work.

References

1. Kennedy, S.H., Lam, R.W., et al., CANMAT Depression Work Group: Canadian Network for Mood and Anxiety Treatments (CANMAT) 2016 Clinical Guidelines for the Management of Adults with Major Depressive Disorder: Section 3. Pharmacological Treatments. Can J Psychiatry. 61, 540–560 (2016).
2. Dusi, N., Barlati, S., et al.: Brain Structural Effects of Antidepressant Treatment in Major Depression. Current Neuropharmacology. 13, 458–465.
3. Stephen, M.S.: Stahl's Essential Psychopharmacology: Neuroscientific Basis and Practical Applications. Cambridge University Press (2013).
4. Zhang, F., Daducci, et al.: Quantitative mapping of the brain's structural connectivity using diffusion MRI tractography: A review. NeuroImage. 249, 118870 (2022).
5. Simona, L., Dogu Baran, A.: Studying topographic organization of the brain with directional derivatives of connectivity. Presented at the ISMRM , New York, NY, USA (2024).
6. Sullivan, J.J., Zekelman, L.R., et al.: Directionally encoded color track density imaging in brain tumor patients: A potential application to neuro-oncology surgical planning. NeuroImage: Clinical. 38, 103412 (2023).
7. Sun, Z., Naismith, S.L., et al.: A novel method for PET connectomics guided by fibre-tracking MRI: Application to Alzheimer's disease. Human Brain Mapping. 45, e26659 (2024).
8. Calamante, F., Tournier, J.-D., et al.: A generalised framework for super-resolution track-weighted imaging. NeuroImage. 59, 2494–2503 (2012).
9. Chen, K.-T.: Integration of Paths--A Faithful Representation of Paths by Noncommutative Formal Power Series. Transactions of the American Mathematical Society. 89, 395–407 (1958).

10. Lyons, T.: Rough paths, Signatures and the modelling of functions on streams. arXiv: Probability. (2014).
11. Xie, Z., Sun, Z., et al.: Learning Spatial-Semantic Context with Fully Convolutional Recurrent Network for Online Handwritten Chinese Text Recognition. IEEE Transactions on Pattern Analysis and Machine Intelligence. 40, 1903–1917 (2018).
12. Yang, W., Jin, L., et al.: Rotation-free online handwritten character recognition using dyadic path signature features, hanging normalization, and deep neural network. In: 2016 23rd International Conference on Pattern Recognition (ICPR). pp. 4083–4088 (2016).
13. Do, C., Manfredo, P.: Differential Geometry of Curves and Surfaces. Prentice-Hall (1976).
14. Kellner, E., Dhital, B., et al.: Gibbs-ringing artifact removal based on local subvoxel-shifts. Magnetic Resonance in Medicine. 76, 1574–1581 (2016).
15. Tustison, N.J., Avants, B.B., et al.: N4ITK: Improved N3 Bias Correction. IEEE Transactions on Medical Imaging. 29, 1310–1320 (2010).
16. Veraart, J., Novikov, D.S., et al.: Denoising of diffusion MRI using random matrix theory. NeuroImage. 142, 394–406 (2016).
17. Jenkinson, M., Beckmann, C.F., et al.: FSL. NeuroImage. 62, 782–790 (2012).
18. Tournier, J.-D., Smith, R., et al.: MRtrix3: A fast, flexible and open software framework for medical image processing and visualisation. NeuroImage. 202, 116137 (2019).
19. Smith, R.E., Tournier, J.-D., et al.: SIFT: Spherical-deconvolution informed filtering of tractograms. NeuroImage. 67, 298–312 (2013).
20. Smith, R.E., Tournier, J.-D., et al.: The effects of SIFT on the reproducibility and biological accuracy of the structural connectome. NeuroImage. 104, 253–265 (2015).
21. Nagao, S.: Pontine nuclei-mediated cerebello-cerebral interactions and its functional role. Cerebellum. 3, 11–15 (2004).
22. Guo, W., Liu, F., et al.: Unidirectionally affected causal connectivity of cortico-limbic-cerebellar circuit by structural deficits in drug-naive major depressive disorder. Journal of Affective Disorders. 172, 410–416 (2015).
23. Damme, K.S.F., Park, J.S., et al.: Depression and Psychosis Risk Shared Vulnerability for Motor Signs Across Development, Symptom Dimensions, and Familial Risk. Schizophrenia Bulletin. 48, 752–762 (2022).
24. Safadi, Z., Grisot, G., et al.: Functional Segmentation of the Anterior Limb of the Internal Capsule: Linking White Matter Abnormalities to Specific Connections. J. Neurosci. 38, 2106–2117 (2018).
25. Zhu, X., Wang, X., et al.: Altered white matter integrity in first-episode, treatment-naive young adults with major depressive disorder: A tract-based spatial statistics study. Brain Research. 1369, 223–229 (2011).
26. Zou, K., Huang, X., et al.: Alterations of white matter integrity in adults with major depressive disorder: a magnetic resonance imaging study. Journal of Psychiatry and Neuroscience. 33, 525–530 (2008).
27. Chen, G., Guo, Y., et al.: Intrinsic disruption of white matter microarchitecture in first-episode, drug-naive major depressive disorder: A voxel-based meta-analysis of diffusion tensor imaging. Progress in Neuro-Psychopharmacology and Biological Psychiatry. 76, 179–187 (2017).
28. Mithani, K., Davison, B., et al.: The anterior limb of the internal capsule: Anatomy, function, and dysfunction. Behavioural Brain Research. 387, 112588 (2020).
29. Seiger, R., Gryglewski, G., et al.: The Influence of Acute SSRI Administration on White Matter Microstructure in Patients Suffering From Major Depressive Disorder and Healthy Controls. International Journal of Neuropsychopharmacology. 24, 542–550 (2021).

30. Ghazi Sherbaf, F., Same, K., et al.: Altered white matter microstructure associated with mild and moderate depressive symptoms in young adults, a diffusion tensor imaging study. NeuroReport. 29, 685 (2018).
31. Liu, Z., Kang, L., et al.: Injuries in Left Corticospinal Tracts, Forceps Major, and Left Superior Longitudinal Fasciculus (Temporal) as the Quality Indicators for Major Depressive Disorder. Neural Plasticity. 2021, 2348072 (2021).
32. Yang, X., Wang, Y., et al.: White matter microstructural abnormalities and their association with anticipatory anhedonia in depression. Psychiatry Research: Neuroimaging. 264, 29–34 (2017).
33. Qin, J., Dong, D., et al.: A Novel Path Signature-Based Metric for Quantifying Morphological Characteristics of White Matter Fibers. International Society for Magnetic Resonance in Medicine. (2025).